J. Astrophys. Astr. (2020) 41:5
https://doi.org/10.1007/s12036-020-9620-3

Simulation of radiation field inside interplanetary spacecraft

G. N. TIMOSHENKO[1,2,*] and I. S. GORDEEV[1,2]

[1]Joint Institute for Nuclear Research, 141980 Dubna, Moscow Region, Russia.
[2]Dubna State University, 141982 Dubna, Moscow Region, Russia.
*Corresponding author. E-mail: tim@jinr.ru

MS received 14 September 2019; accepted 24 November 2019; published online 27 February 2020

Abstract. A simulation of the radiation field inside a habitable module (a diameter of 6 m and length of 12 m) of a spacecraft generated by isotropic Galactic Cosmic Radiation (GCR) in deep interplanetary space is carried out for minimum and maximum solar activity using the FLUKA code. Protons, alpha-particles, deuterons, ^{3}He, and nuclei with $Z > 2$ are considered as primary GCR irradiating the spacecraft isotropically. The following particles are included in FLUKA radiation transport through the module shell (15 g/cm^2 of Al): protons, neutrons, γ-rays, electrons, $\pi^{\pm}$-mesons, $\mu^{\pm}$-mesons d, t, and nuclei from He to Ni. The inner particle spectra are needed to assess the astronaut's radiation risk in a long-term interplanetary mission.

Keywords. Galactic cosmic radiation—astronaut exposure to space radiation—spacecraft radiation shield—FLUKA code—simulation of nucleus–nucleus interaction—radiation transport through matter.

1. Introduction

Astronauts traveling on a protracted voyage to Mars will be exposed mainly to the secondary radiation originated from Galactic Cosmic Radiation (GCR) interacted with spacecraft shell. Due to the high energy of GCR, a spacecraft shell is not a barrier for them and part of the primary particles can penetrate the shell without nuclear interactions. Other particles and nuclei of the GCR generate in the shell numerous secondary particles and nuclear fragments with a very wide energy range. The mixed non-directional radiation field inside the spacecraft varies with solar activity (SA) both in composition and in the energy spectra of the field components. The inner field has practically the same composition as the composition of the GCR in space, but as a result of GCR interaction with the spacecraft matter, unstable particles (neutrons, mesons, short- and mid-life nuclei) appear that are not present in the GCR. Therefore, a complete calculation of the spectra of all the secondary particles forming the radiation field inside the spacecraft is very complicated and time-consuming.

Despite the abundance of predictions of astronaut doses due to the GCR, detailed information on the components of the internal field depending on the SA is not practically available. The reason for this is the fact that NASA uses the HZETRN code for estimating the dose of astronauts, which does not require the calculation of the spectra of particles in the internal radiation field inside the spacecraft. The HZETRN is a deterministic transport code specifically developed by NASA for space radiation transport. It employs numerical solutions of the Boltzmann equation. The decisive advantage of this code is that it does not require a lot of time. In combination with an anthropomorphic phantom, it allows one to calculate radiation doses in a phantom from particles that have passed through the spacecraft shell without intermediate calculations of their spectra. However, the interest to fluence based approaches to radiation risk assessment demand a higher degree of accuracy from the code, comparable to the accuracy that transport Monte Carlo (MC) computer codes can provide. Some estimations of the field inside the spacecraft have been made earlier on the basis of various programs of radiation transport in the matter (see, for example, Heilbronn *et al*. 2015; Aghara *et al*. 2009; Pham & El-Genk 2013; De Wet & Townsend 2017). Most of these calculations were made in a simplified "source-shield" geometry, in which the spacecraft shell was imitated either by a flat slab or a sphere of small diameter that is very different from the real geometry of the future spacecraft. Often,

from the entire ensemble of GC particles, only the main components were taken into account, the same was in the inner radiation field. In reality, the radiation field that astronauts will be exposed in the spacecraft is very complex. The most complete comparisons of calculations of the radiation fields behind a spacecraft shell by HZETRN, SHIELD, FLUKA and GEANT4 codes were made in Norbury *et al.* (2017). Comparisons were made for spectra of neutrons, light ions ($Z \leq 2$), heavy ions ($Z > 2$) and pions emitted from the aluminium flat target irradiated by a narrow beam of GC particles. Of course, the calculated particle spectra are difficult to interpret as the real spectra of particles inside the spacecraft, but even with this, serious discrepancies between the HZETRN and MC codes are found, especially below the several hundred MeV region.

In this paper, we have made efforts to obtain as close as possible to reality the energy fluences of particles in the internal field of the spacecraft, irradiated by the GCR in interplanetary space. The correctness of the performed calculations is determined not by the statistical errors of the calculations, but by the initial data on the spectra of the GCR depending on the SA and the accuracy of the nuclear interaction simulation by the FLUKA code. The results of the work can also be used to estimate the dose of astronauts during interplanetary flights by fluence based approaches to radiation risk assessment.

2. GCR simulation and spacecraft geometry

Timoshenko *et al.* (2017) presented the results of our calculation by the MCNPX 2.6.0 code of some light components (p, n, γ, π- and K-mesons, deuterons, tritons, ^{3}He and alpha-particles) in the inner radiation field for the chosen variant of the spacecraft habitable module (cylinder with a diameter of 6 meters and length of 12 meters and the aluminium shell with a thickness of 15 g/cm^2). These dimensions of the habitable module slightly exceeded the dimensions of the ISS modules, taking into account the longer duration of the flight. It was assumed that the habitable module will be a dwelling where astronauts will spend most of their time. The proposed thickness of the module shell is greater than the average thickness of the ISS shell because it must provide protection when passing through the radiation belt of the Earth and from solar radiation outside the Earth's magnetosphere.

The spectra of isotropic GCR particles were calculated by the algorithm (Matthia *et al.* 2013) for mean Wolf numbers $W = 0$ and 190 (corresponding to an acceptable minimum and maximum solar activity). The initial GCR were protons and alpha-particles within the energy range of 10–10^5 MeV/n, because only near 1% of GCR are nuclei with $Z > 2$. The overwhelming proportions of all protons and alphas (95–97%) were found in this energy range. The habitable module was filled with dry air at normal pressure.

In the previous article by Timoshenko *et al.* (2017), the spectra of the following components of the internal radiation field averaged over the entire volume of the module were presented: protons, neutrons, π-mesons and alpha particles. The low energy threshold for all charged particles was 10 Mev/n; for neutrons −1 MeV. This is due to the neutron component below 1 MeV which depends more on the specific filling of the module with various hydrogen-containing materials than on the GCR spectra.

In the present article, we extended past calculations to all GCR up to nickel nuclei, in order to be able to estimate the astronaut doses over the flight period from all components of the internal field. New calculations, presented in the current article, were performed using the FLUKA-2011.2x.6 code, often used for space applications (Ferrari *et al.* 2001a, b; Andersen *et al.* 2004).

3. Verification method of inner radiation field simulation

FLUKA is a multiparticle transport code capable of handling hadronic and electromagnetic cascades up to very high energies (100 TeV), widely used for radioprotection. In FLUKA, a relativistic Quantum Molecular Dynamics (QMD) model RQMD-2.4 is applied successfully to relativistic nucleus−nucleus collisions simulation over a wide energy range, from ≈0.1 GeV/n up to several hundreds of GeV/n. The high energy nucleus–nucleus collisions in FLUKA is successfully covered by DPMJET (event generator in FLUKA based on the Dual Parton Model in connection with the Glauber formalism to simulate nucleus interactions at an accelerator and cosmic ray energies up to 10^9 GeV/n). It is possible to take into account the electromagnetic dissociation of the projectile nucleus or target nucleus in the Coulomb field. The electromagnetic contribution dominates in interactions of ultra-relativistic nuclei leading to small changes in the charge $\Delta Z = 0, -1, -2$.

The calculations of the spectra of the internal charged particles from GC protons and alpha particles, performed earlier by MCNPX 2.6.0 (Timoshenko *et al.*

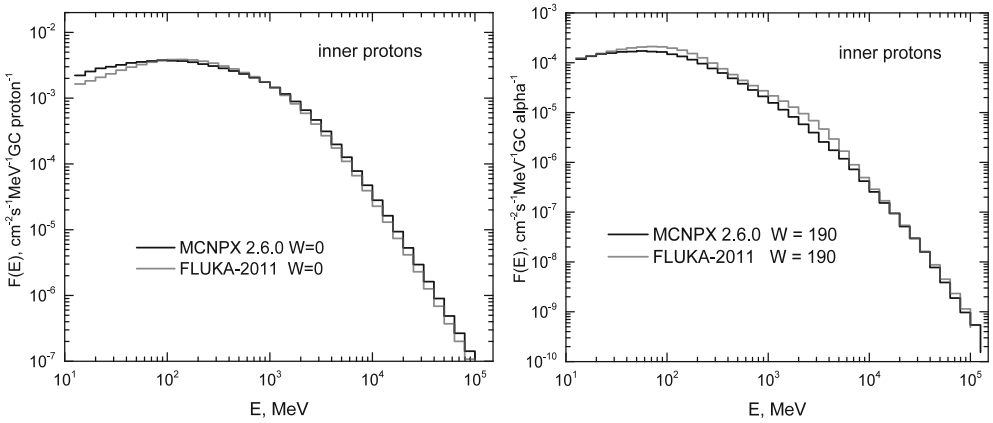

Figure 1. Comparison of calculations of the spectra of internal protons from protons and alpha particles of GCR behind the 15 g/cm^2 Al shell of the spacecraft module, performed by MCNPX and FLUKA.

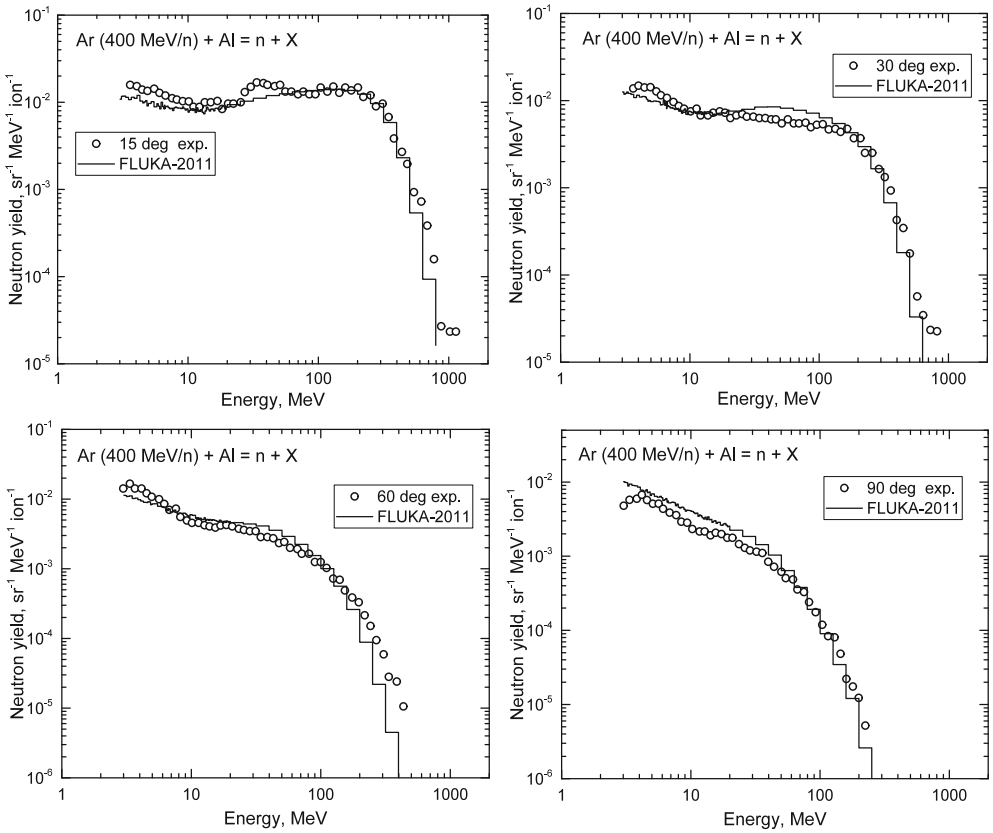

Figure 2. The results of the simulation of the experiment (Kurosawa *et al*. 2000) on the measurement of double differential neutron yields from Al target with a thickness of 15 g/cm^2, irradiated with 400 MeV/n Ar nuclei by the FLUKA code.

2017) and new FLUKA-2011 calculations are in good agreement with each other (Figure 1 shows inner proton spectra from GC protons and alpha-particles at minimum and maximum SA, for example). However, in the spectra of secondary neutrons in the range of energy less than 100 MeV, FLUKA gives underestimated results in comparison with MCNPX. This fact has been noted repeatedly in the works of other authors. To check the accuracy of secondary neutrons calculation by FLUKA, a comparison was made with the experiment (Kurosawa *et al*. 2000) (see Figure 2). The agreement of the calculations with the experimental data is quite satisfactory.

Finally, due to the fact that FLUKA and MCNPX give slightly different results, especially for neutrons, the old data (Timoshenko *et al*. 2017) from protons and

alpha particles of the GCR were also recalculated using the FLUKA code.

Due to the large relative biological effectiveness (RBE) of heavy nuclei, their doses are significant despite their small fluences in the GCR. For this reason, it is very important to correctly simulate the fragmentation of projectile nuclei in the peripheral nucleus−nucleus collisions in addition to the processes of generation due to numerous secondary particles in central collisions. Peripheral nucleus−nucleus collisions characterized by large impact parameters lead mainly to fragmentation reactions of the projectiles and the target nucleus, as a result of which the fragments of the projectiles will move at almost its former speed, and the target fragments will have low excitation energy, going to the evaporation of nucleons and light nuclei.

To check the RQMD operation, the comparison of fragment charge cross sections for 1.05 GeV/n Fe ions on Al with the experimental data (Zeitlin *et al.* 1997) was done. These experimental date corresponds to the energy near the peak of the solar-modulated GCR iron energy spectrum. The results of the comparison together with old FLUKA-2003 calculation are presented in Figure 3. It can be seen that the results for FLUKA-2011 are in better agreement with the experiment in comparison with the calculation for FLUKA-2003, especially in the field of reactions with the emission of one or two nucleons, caused not only by the strong interaction but also by the possible electromagnetic dissociation of the projectiles in the Coulomb field.

Thus, in the internal cavity of the spacecraft, the heavy GC nuclei will produce nucleons of a wide energy spectrum, secondary nuclei-fragments with practically the same energy per nucleon as the primary projectile GC nuclei, and a few light nuclei-fragments from the target nuclei. In Figure 4, the yields of secondary protons, alpha-particles, Li and Be fragments from ^{27}Al target 15 g/cm^2 thickness bombarded by ^{56}Fe (5 GeV/n) are presented for narrow forward- angular cone ($0 \pm 5°$) and forward hemisphere ($0 \pm 90°$). It can be seen that the evaporative nucleons from the target make a significant contribution to the total yield of the nucleons. As for the secondary nuclei, the excitation energy is enough to evaporate even light nuclei (^{4}He, Li) from the target, but the heavier fragments (Be) are due only to the fragmentation of the projectile. With the growth of the projectile energy, the fraction of evaporation fragments from the target and their Z increases, while fragmentation of a projectile nucleus is weakly dependant on its energy (limiting fragmentation). From Figure 4, it is also seen that the

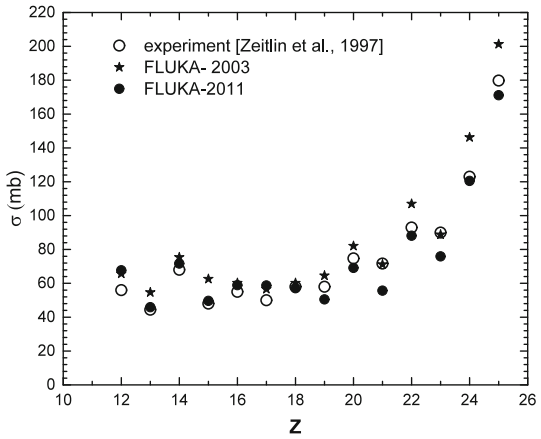

Figure 3. Fragment charge cross sections for 1.05 GeV/n Fe ions on Al target.

energy of fragments per nucleon can exceed the energy per nucleon of the primary projectile nucleus due to the cumulative effect of fragmentation (especially for nucleons).

4. Results of the inner radiation field simulation by FLUKA code

In the present work, deuterons, ^{3}He and nuclei with $2 < Z < 28$ in the energy range of $10-10^5$ MeV/n were considered as primary GC particles in addition to protons and alpha particles. The spectra of GC protons and alpha-particles simulated by the algorithm (Matthia *et al.* 2013) for $W = 0$ and 190 are presented in Figure 5. The experiments (Myers *et al.* 2005; Adriani *et al.* 2016) show that the fluence of deuterons in the primary GCR is very small ($\sim 2-2.5\%$ to protons fluence) and owing to GC deuterons, they have a secondary nature. Primary ^{2}H and ^{3}He spectra may be presented as (Cucinotta *et al.* 2006) (here E is in MeV/n):

$$^3\mathrm{He}(E) = 0.0764 + 0.097\ \exp[-0.5(\ln(E/1660)/1306)^2]\,{}^4\mathrm{He}(E);$$
$$^2\mathrm{H}(E) = 0.2\,{}^4\mathrm{He}(E).$$

Only the most abundant GC nuclei were considered at GCR interaction with the spacecraft shell for each element. It can lead to little errors in the description of both primary nuclei attenuation and secondary particle production including high-energy neutron production from the many neutron-rich isotopes that occur. However, for heavy nuclei, the error in the yield of secondary neutrons due to this assumption will be insignificant. There is a significant difference in the yield of secondary neutrons only between GC protons and deuterons.

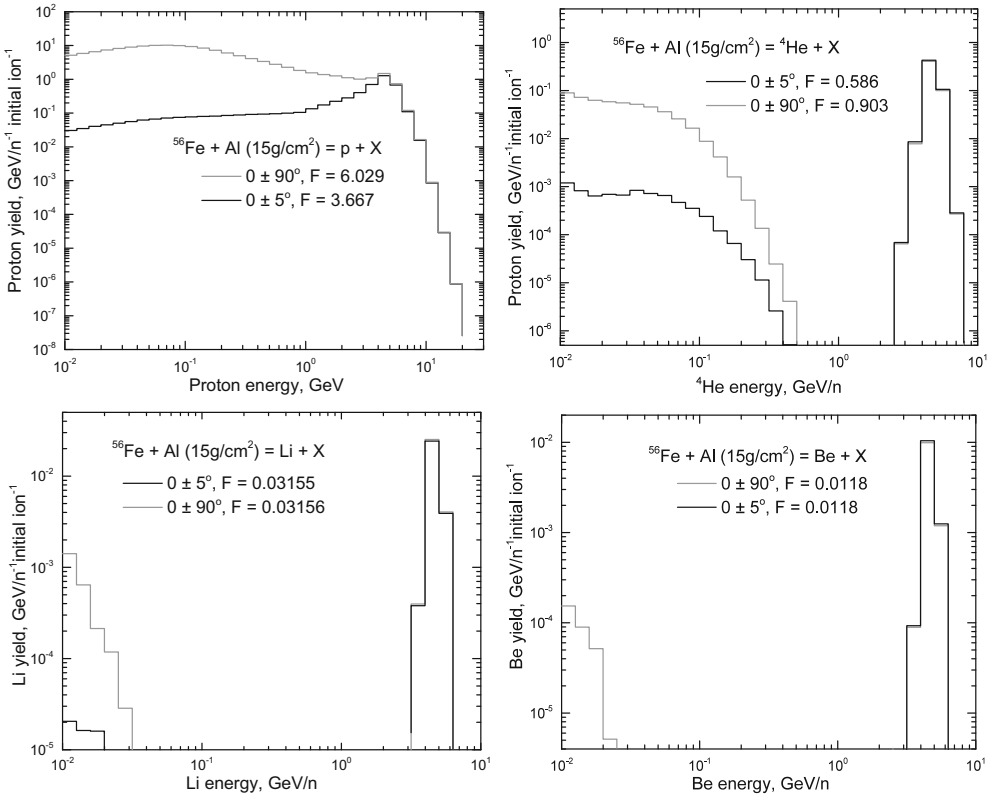

Figure 4. The proton, ^{4}He, Li and Be fragments yield in the forward direction and in the hemisphere at the interaction of Fe nuclei (5 GeV/n) with Al target (15 g/cm^2).

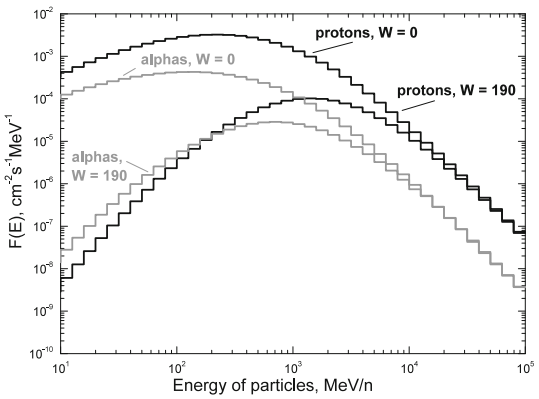

Figure 5. Energy spectra of initial GC protons and alpha-particles at minimum and maximum SA.

The big volume of all secondary components inner spectra calculation from GCR was carried out on the base of HybriLIT heterogeneous computing platform (LIT, JINR) (Adam *et al*. 2018). The statistical accuracy of the calculations provided a 10% error in the region of maximum particle energies. The spectra of secondary particles from all GCR were then summarized and the result was then normalized to the GCR total fluence depending on SA and particle abundance. The inner summarized spectra of some particles are shown in Figure 6.

The fluence rates of outer GCR and inner particles are presented in Table 1 for comparison. The energy range for neutrons and gamma-rays is spread from 1 to 10^5 MeV/n, for charged particles – from 10–10^5 MeV/n.

It is noteworthy that the fluence rate of the main component of the internal field — protons — exceeds the fluence rate of the primary protons of the GCR. A similar situation is observed with respect to the light nuclei Li and Be since the main part of them is formed due to the fragmentation of the heavier nuclei GCR. This also explains the difference in GCR relative abundances compared with the solar system ones.

Protons and secondary neutrons and gamma-rays make the largest contribution to the total fluence in the radiation field inside the module. In principle, the calculation of neutron and gamma-ray doses according to the data of this work will give underestimated results due to the energy threshold of 1 MeV (gamma-rays from thermal neutron capture are also not taken into account).

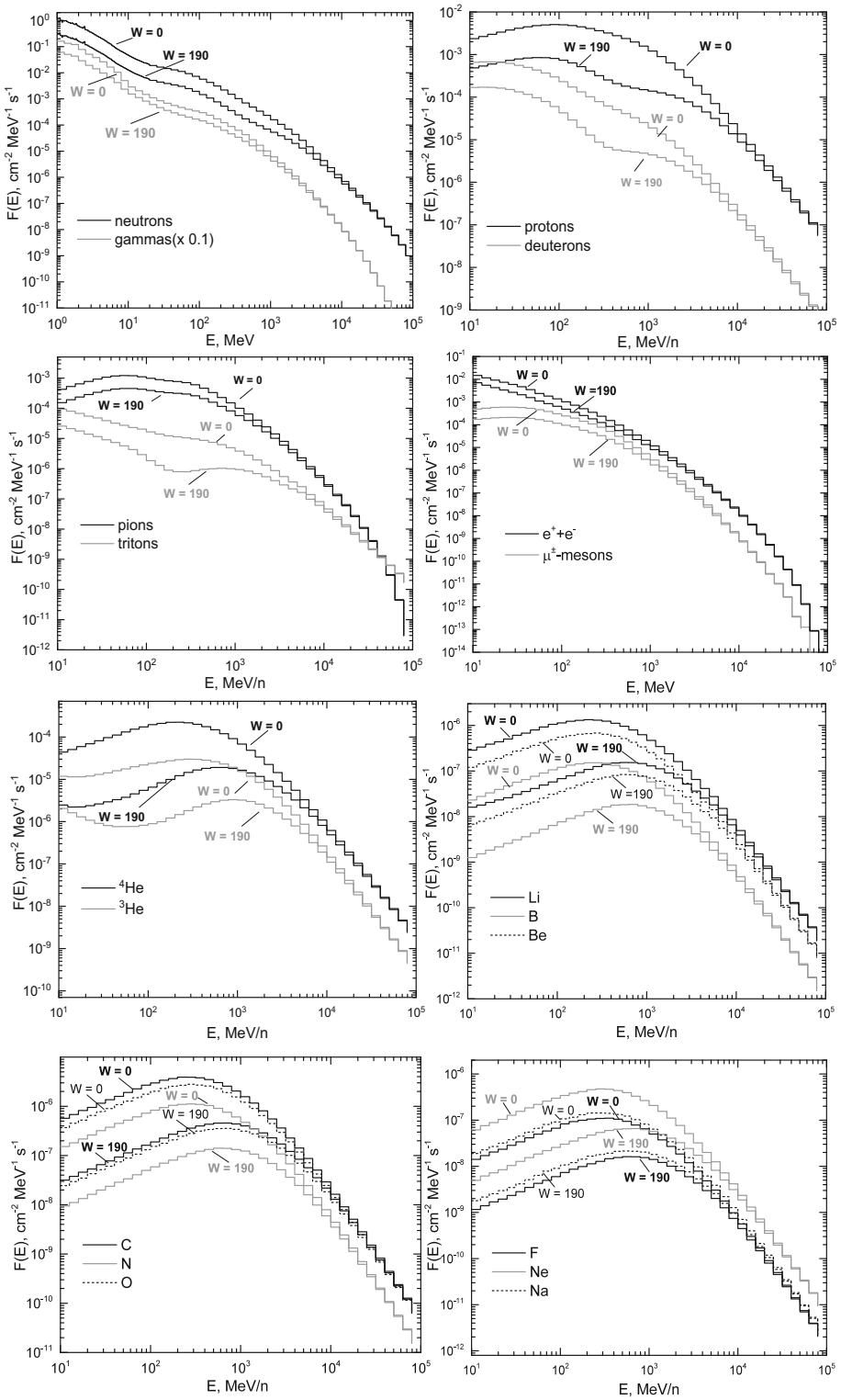

Figure 6. Energy spectra of components of inner radiation field inside the habitable module with 15 g/cm^2 Al shell at minimum and maximum SA.

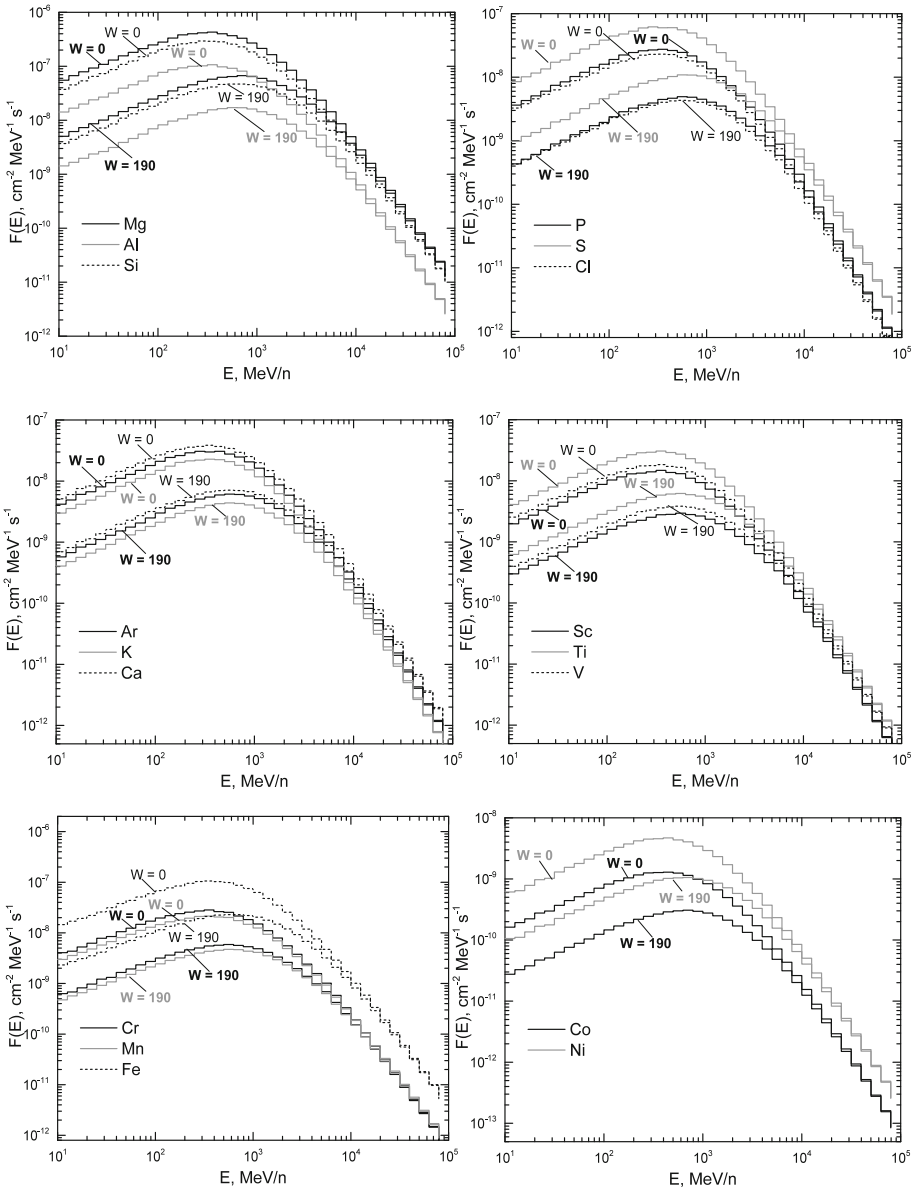

Figure 6. *Continued.*

But the realistic calculation of the soft parts of the energy spectra of neutrons and gamma-rays is not possible without taking into account the specific filling of the module with equipment, partitions, instruments, etc. The presence of muons in the internal field is mainly due to the decay of pions. We did not take into account GC electrons (∼1% of the total fluence rate of the hadrons of the GCR). GC electrons are subject to effective energy loss on their way owing to bremsstrahlung and synchrotron radiation, Compton scattering and ionization. They are also very sensitive to the magnetic field, which prevents them from penetrating deep into the solar system. Therefore, the electrons with energy above 10 MeV in the table are mainly due to the electromagnetic cascade from high-energy gamma-rays.

As a result, the total fluence rate of different types of radiation inside the habitable module with a shell of 15 g/cm^2 Al is almost three times larger than the total fluence rate of GCR in the minimum SA and nearly six times in the maximum SA.

The presence of ship protection also leads to a decrease in the variability of the internal field depending on the SA in comparison with the GCR. The relationship between the fluence rates of the primary GC particles and the particles of the internal field is shown in Figure 7.

Table 1. Comparison of the external GCR fluence rates and the fluence rates of internal field particles ($cm^{-2}\,s^{-1}$) at the minimum and maximum SA.

Particle	GCR fluence rate $W = 0$	Inner fluence rate $W = 0$	GCR fluence rate $W = 190$	Inner fluence rate $W = 190$
Protons	4.499	**4.695***	0.566	**0.802**
Neutrons	–	4.571	–	1.24
Gammas	–	4.349	–	1.66
Electrons+positrons	–	**0.507**	–	**0.245**
$\pi^{\pm}$-mesons	–	0.582	–	0.274
$\mu^{\pm}$-mesons	–	$8.42 \cdot 10^{-2}$	–	$3.39 \cdot 10^{-2}$
$K^{\pm}$-mesons	–	$4.5 \cdot 10^{-3}$		$3 \cdot 10^{-3}$
Deuterons	$8.3 \cdot 10^{-2}$	$\mathbf{1.21 \cdot 10^{-1}}$	$1.69 \cdot 10^{-2}$	$\mathbf{2.90 \cdot 10^{-2}}$
Tritons	–	$1.64 \cdot 10^{-2}$	–	$4.205 \cdot 10^{-3}$
^{3}He	$5.77 \cdot 10^{-2}$	$4.78 \cdot 10^{-2}$	$1.27 \cdot 10^{-2}$	$1.17 \cdot 10^{-2}$
Alpha-particles	0.415	0.246	$8.46 \cdot 10^{-2}$	$5.63 \cdot 10^{-2}$
Li	$1.61 \cdot 10^{-3}$	$\mathbf{1.64 \cdot 10^{-3}}$	$3.68 \cdot 10^{-4}$	$\mathbf{4.49 \cdot 10^{-4}}$
Be	$8.91 \cdot 10^{-4}$	$8.54 \cdot 10^{-4}$	$2.00 \cdot 10^{-4}$	$\mathbf{2.35 \cdot 10^{-4}}$
B	$3.23 \cdot 10^{-3}$	$1.91 \cdot 10^{-3}$	$7.02 \cdot 10^{-4}$	$5.10 \cdot 10^{-4}$
C	$1.15 \cdot 10^{-2}$	$5.22 \cdot 10^{-3}$	$2.39 \cdot 10^{-3}$	$1.42 \cdot 10^{-3}$
N	$3.02 \cdot 10^{-3}$	$1.53 \cdot 10^{-3}$	$6.34 \cdot 10^{-4}$	$4.20 \cdot 10^{-4}$
O	$1.06 \cdot 10^{-2}$	$3.98 \cdot 10^{-3}$	$2.29 \cdot 10^{-3}$	$1.15 \cdot 10^{-3}$
F	$2.48 \cdot 10^{-4}$	$1.63 \cdot 10^{-4}$	$5.95 \cdot 10^{-5}$	$4.97 \cdot 10^{-5}$
Ne	$1.85 \cdot 10^{-3}$	$6.80 \cdot 10^{-4}$	$3.82 \cdot 10^{-4}$	$2.03 \cdot 10^{-4}$
Na	$4.36 \cdot 10^{-4}$	$2.08 \cdot 10^{-4}$	$8.71 \cdot 10^{-5}$	$6.41 \cdot 10^{-5}$
Mg	$2.02 \cdot 10^{-3}$	$6.90 \cdot 10^{-4}$	$4.82 \cdot 10^{-4}$	$2.23 \cdot 10^{-4}$
Al	$4.08 \cdot 10^{-4}$	$1.65 \cdot 10^{-4}$	$9.11 \cdot 10^{-5}$	$5.32 \cdot 10^{-5}$
Si	$1.75 \cdot 10^{-3}$	$4.78 \cdot 10^{-4}$	$3.83 \cdot 10^{-4}$	$1.56 \cdot 10^{-4}$
P	$8.46 \cdot 10^{-5}$	$4.34 \cdot 10^{-5}$	$1.90 \cdot 10^{-5}$	$1.45 \cdot 10^{-5}$
S	$3.49 \cdot 10^{-4}$	$1.03 \cdot 10^{-4}$	$7.74 \cdot 10^{-5}$	$3.46 \cdot 10^{-5}$
Cl	$7.59 \cdot 10^{-5}$	$3.65 \cdot 10^{-5}$	$1.69 \cdot 10^{-5}$	$1.24 \cdot 10^{-5}$
Ar	$1.38 \cdot 10^{-4}$	$4.96 \cdot 10^{-5}$	$3.33 \cdot 10^{-5}$	$1.74 \cdot 10^{-5}$
K	$1.02 \cdot 10^{-4}$	$3.61 \cdot 10^{-5}$	$2.21 \cdot 10^{-5}$	$1.22 \cdot 10^{-5}$
Ca	$2.57 \cdot 10^{-4}$	$6.26 \cdot 10^{-5}$	$5.06 \cdot 10^{-5}$	$2.17 \cdot 10^{-5}$
Sc	$5.08 \cdot 10^{-5}$	$2.29 \cdot 10^{-5}$	$1.06 \cdot 10^{-5}$	$8.21 \cdot 10^{-6}$
Ti	$1.72 \cdot 10^{-4}$	$4.80 \cdot 10^{-5}$	$3.59 \cdot 10^{-5}$	$1.72 \cdot 10^{-5}$
V	$9.04 \cdot 10^{-5}$	$2.94 \cdot 10^{-5}$	$1.88 \cdot 10^{-5}$	$1.09 \cdot 10^{-5}$
Cr	$1.81 \cdot 10^{-4}$	$4.62 \cdot 10^{-5}$	$3.68 \cdot 10^{-5}$	$1.71 \cdot 10^{-5}$
Mn	$1.14 \cdot 10^{-4}$	$3.88 \cdot 10^{-5}$	$2.61 \cdot 10^{-5}$	$1.51 \cdot 10^{-5}$
Fe	$1.18 \cdot 10^{-3}$	$1.97 \cdot 10^{-4}$	$2.75 \cdot 10^{-4}$	$7.71 \cdot 10^{-5}$
Co	$9.28 \cdot 10^{-6}$	$2.67 \cdot 10^{-6}$	$2.65 \cdot 10^{-6}$	$1.10 \cdot 10^{-6}$
Ni	$5.45 \cdot 10^{-5}$	$9.20 \cdot 10^{-6}$	$1.37 \cdot 10^{-5}$	$3.68 \cdot 10^{-6}$
Total	5.094	**15.238**	0.689	**4.366**

*There are cases of exceeding the fluence rate of the inner particles over the fluence rate of the outer particles, which are shown in bold font.

On average, the attenuation of heavy nuclei by the spacecraft shell is nearly two times while the number of protons and light nuclei increases.

Thus, the proportion of heavy nuclei with large RBE in the internal field decreases, which compensates the total increase of the internal field particle fluence at estimating the astronaut dose. The spacecraft shell also leads to a decrease in the variability of the internal field depending on the SA in comparison with the GCR.

Variations in the composition of the internal field as a function of SA are shown in Figure 8. The main changes are the reduction in the proton portion and the increase in the gamma-ray portion with an increase of SA.

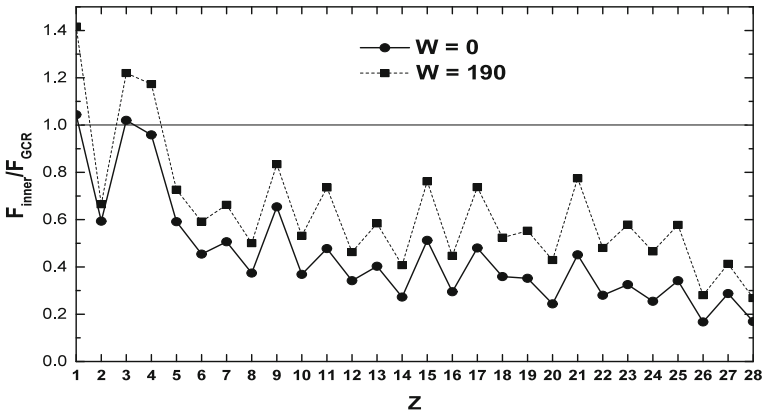

Figure 7. The ratio between inner field particle fluence rates and initial GCR fluence rates at minimum and maximum SA.

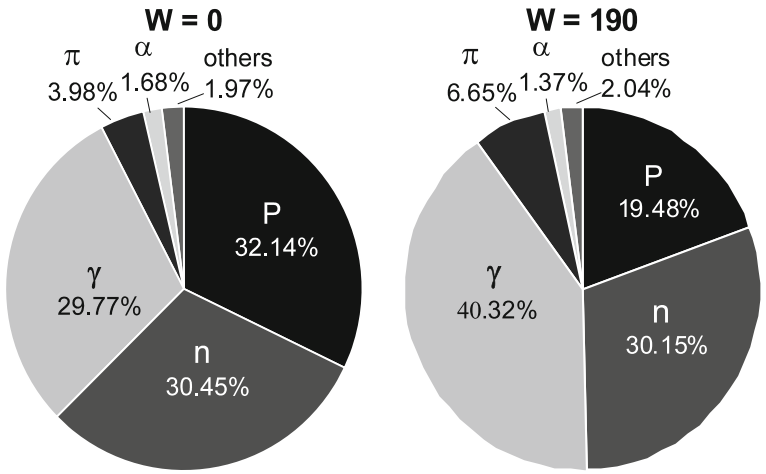

Figure 8. Variations in the composition of the internal radiation field depending on SA.

5. Conclusion

It should be noted that for a number of reasons, the calculated internal field can be slightly underestimated (first of all, due to the accepted energy threshold of neutrons and gamma quanta). Nevertheless, the detailed calculation of the internal radiation field behind the realistic shell of a spacecraft given in this work can be a basis for estimating the astronaut dose during long-term interplanetary flights by the fluence-based approach. In this case, the effective dose equivalent can be calculated with the inner particle energy spectra and appropriate fluence-to-effective dose equivalent conversion coefficients.

References

Adam Gh., Bashashin M., Belyakov D., Kirakosyan M., Matveev M., Podgainy D., Sapozhnikova T., Streltsova O., Torosyan Sh., Vala M., Valova L., Vorontsov A., Zaikina T., Zemlyanaya E., Zuev M. 2018, ITecosystem of the HybriLIT heterogeneous platform for high performance computing and training of ITspecialists, Selected Papers of the 8th International Conference on "Distributed Computing and Grid-Technologies in Science and Education" (GRID 2018), Dubna, Russia, September 10–14, 2018, CEUR-WS.org/Vol2267

Adriani O., Barbarino G. C., Bazilevskaya G. A., Bellotti R. *et al*. 2016, Astrophys. J., 818(1), 1

Aghara S. K., Blattnig S. R., Norbury J. W., Singleterry R. C. 2009, Nuclear Instrum. Methods Phys. Res., B267, 1115

Andersen A., Ballarini F., Battistoni G., Campanella M., Carboni M., Cerutti F., Empl A., Fass A., Ferrari A., Gadioli E., Garzelli M. V., Lee K., Ottolenghi A., Pelliccioni M., Pinsky L. S., Ranft J., Roesler S., Sala P. R., Wilson T. L. 2004, Adv. Space Res., 34, 1302

Cucinotta F. A., Wilson J. W., Saganti P., Hu X., Kim M.-H. Y., Cleghorn T., Zeitlind C., Tripathi R. K. 2006, Radiat. Meas., 41, 1235

De Wet W. C., Townsend L. W. 2017, Life Sci. Space Res., 14, 51

Ferrari A., Ranft J., Sala P. 2001, Phys. Med., 17(Suppl. 1), 72

Ferrari A., Pelliccioni M., Rancati T. 2001, Radiat. Prot. Dosim., 93(2), 101

Heilbronn L. H., Borak T. B., Townsend L. W., Tsai Pi-En, Burnham C. A., McBeth R. A. 2015, Life Sci. Space Res., 7, 90

Kurosawa T., Nalao N., Nakamura T., Iwase H., Sato H., Uwamino Y., Fukumura A. 2000, Phys. Rev. C, 62, 044615-1

Matthia D., Berger T., Mrigakshi A. I., Reitz G. 2013, Adv. Space Res., 51, 329

Myers Z. D., Seo E. S., Wang J. Z., Alford R. W., Abe K., Anraku K. *et al*. 2005, Adv. Space Res., 35(1), 151

Norbury J. W., Slaba T. C., Sobolevsky N., Reddell B. D. 2017, Life Sci. Space Res., 14, 64

Pham T. T., El-Genk M. S., 2013, Simulations of space radiation interactions with materials and dose estimates for a lunar shelter and aboard the international space station, Technical Report ISNPS-UNM-1-2013, Institute for Space and Nuclear Power Studies (ISNPS), University of New Mexico

Timoshenko G. N., Krylov A. R., Paraipan M., Gordeev I. S. 2017, Radiat. Meas., 107, 27

Zeitlin C., Heilbronn L., Miller J. *et al.* 1997, Phys. Rev. C56, 388